NANO LETTERS

pubs.acs.org/NanoLett Letter

Giant Second Harmonic Generation by Photoinduced Phase Engineering

Xinyue Li, Boqin Song, Jiahao Yan, Haijun Cao, Tongtong Xue, Jing Chen, Yunyun Dai, Luojun Du, Qinghua Zhang, Sheng Meng, Jian-gang Guo,* Tianping Ying,* and Xiaolong Chen*

Cite This: *Nano Lett.* 2025, 25, 5821−5827 Read Online

ACCESS | Metrics & More | Article Recommendations | Supporting Information

ABSTRACT: Addressing the growing demand for ever-shrinking nonlinear optical devices requires a paradigm shift to two-dimensional (2D) materials to bypass phase-matching limitations encountered in bulk crystals. While strategies like strain, electrical gating, and surface decoration have been explored to enhance the nonlinear susceptibility of 2D materials, the potential of laser-driven effects, with its exceptional controllability and accessibility, remains largely underexplored. Here, we demonstrate an optical approach to achieve a giant second-order parametric response in a metastable noncentrosymmetric 1M-WS_2 by selectively controlling laser pulse duration. We report a record effective second harmonic generation coefficient of ∼2000 pm/V, surpassing typical values of conventional nonlinear crystals by several orders of magnitude. Detailed analyses reveal that the structural distortions unique to the 1M phase are crucial for the enhanced nonlinear response. These findings establish an alternative way to amplify nonlinear optical properties and set 1M-WS_2 as a promising candidate for compact optical modulators and nanolasers.

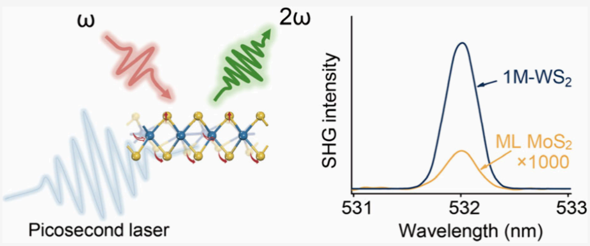

KEYWORDS: *Nonlinear optical response, Second harmonic generation (SHG), Photoinduced phase transition, Two-dimensional material*

Second harmonic generation (SHG), describing the doubling of light frequencies, is a fundamental nonlinear optical phenomenon central to both classical and modern optics, and serves as a powerful probe for symmetry-related phenomena that are otherwise challenging to access.[1−7] While bulk crystals have long been the go-to choice for achieving high energy conversion, their reliance on stringent phase-matching conditions and sufficient light-matter interaction volume severely limits their integration into miniaturized optical devices. Noncentrosymmetric two-dimensional (2D) materials have emerged as a compelling alternative, offering seamless compatibility for on-chip integration and high nonlinear susceptibilities due to their confined electronic states and reduced electric screening.[8−13] Recent efforts have explored various strategies to further enhance their optical performance, including strain engineering,[14−16] electrical gating,[15,17] resonant absorption,[18] and twist phase matching.[19−22]

Laser irradiation serves as a versatile and powerful tool for tuning material properties with exceptional spatial and temporal precision. By leveraging intense light-matter interactions and ultrafast excitation, lasers can induce magnetic moments,[23−25] enhance ferroelectricity,[5,26−29] and drive transient superconducting states.[30−32] With sufficient energy input, photoexcited lattice dynamics can lead to permanent atomic dislocation or even create new kinds of materials.[33−35] This is especially true in 2D materials for their wealth of isomers compared to 3D counterparts. Notable examples include the transformation of MoS_2 from the metallic 1T' phase to the semiconducting 2H phase via laser irradiation, significantly altering its electrocatalytic performance,[36] and photoinduced multistage phase transitions in Ta_2NiSe_5, accompanied by dramatically enhanced electrical conductivity.[37] Despite these remarkable achievements, the study of photoinduced nonlinear responses in 2D materials remains largely untapped.

Here, we report the realization of photoinduced giant SHG response in a novel metastable 1M-WS_2 phase, along with an interesting light-intensity-selective phase transition pathway. As far as we know, this metastable 1M-WS_2 phase is reported for the first time. Previous studies have shown that light irradiation or thermal treatments can transform the metastable 2M-WS_2 phase to a centrosymmetric 2H phase without nonlinear optical response (Figure 1). Our initial motivation was to explore an alternative pathway using lower-intensity light, such as picosecond laser pulse, to introduce other isomeric structures, for example the noncentrosymmetric 3R-WS_2 with comparable energy scale and symmetry-guaranteed

Received: January 24, 2025
Revised: March 10, 2025
Accepted: March 24, 2025
Published: March 26, 2025

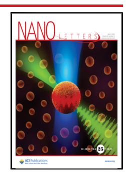

https://doi.org/10.1021/acs.nanolett.5c00536
Nano Lett. 2025, 25, 5821−5827

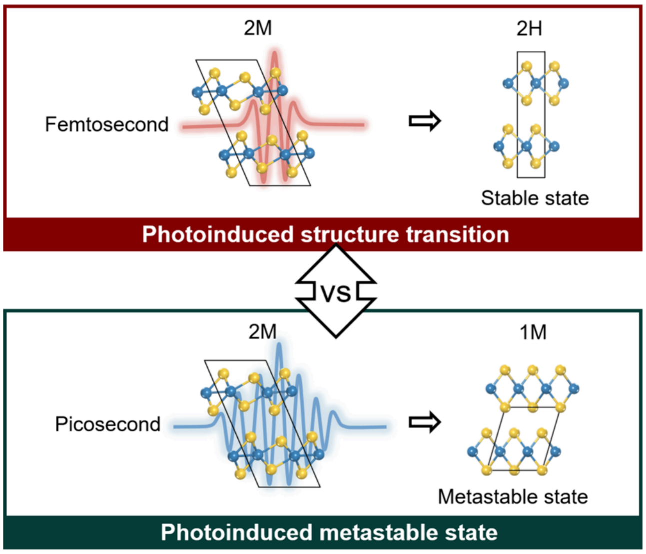

Figure 1. Strategies for photoinduced phase transition. Top panel: Femtosecond laser irradiation induces a structural transition from the 2M phase of WS_2 to the stable 2H phase.[35] Bottom panel: An alternative pathway to the metastable 1M-WS_2 using picosecond laser irradiation. Blue and yellow spheres represent W and S atoms, respectively.

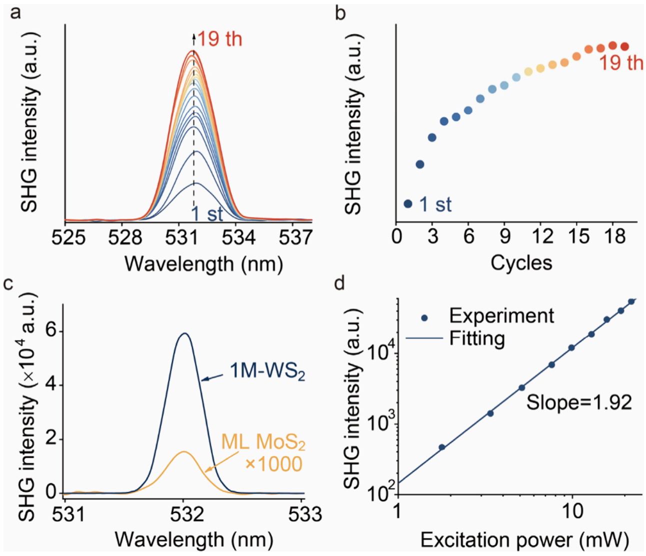

Figure 2. Photoinduced giant SHG response. (a) SHG spectra of 1M-WS_2 with successive laser irradiation cycles. (b) Corresponding SHG intensity in (a) as a function of the number of laser irradiation cycles. (c) SHG spectra of a 3-layer 1M-WS_2 (~2.2 nm) and MoS_2 monolayer under λ_{ex} = 1064 nm. The intensity of ML MoS_2 is scaled by a factor of 1000 for comparison. (d) Excitation power dependence of SHG intensity. Dots are experimental results, and the curve shows a linear fit of the log−log plot with a slope of 1.92.

nonlinear responses. Unexpectedly, we observed an exceptionally high SHG susceptibility of 2362 pm/V, an order of magnitude larger than that of chemical vapor deposition (CVD)-grown 3R-WS_2[38] and comparable to the best-known 2D nonlinear materials. This remarkable enhancement points to the formation of a novel crystal structure, which is further confirmed through detailed structural analyses and theoretical calculations. Additionally, the acquired 1M phase exhibits exceptional air stability and water resistance, rendering it highly suitable for practical applications without the need of passivation.

The experimental setup is straightforward, following the conventional SHG detection method using a 1064 nm laser to trigger both the phase transition and SHG measurement. It is important to note that the phase transition occurs only when the laser pulse energy exceeds 200 μJ (Figure S1). To confirm the persistence of the SHG response, a lower laser energy was used. No appreciable property decline can be observed within a few days after the photoinduced phase transformation, indicating the robustness of the acquired metastable phase. SHG spectra were measured *in situ* every 50 s, with each measurement representing one cycle. Figure 2a shows the SHG intensity of a bulk sample as the number of cycles increases. The peak values for each cycle are extracted in Figure 2b. The SHG intensity increases rapidly during the first few cycles and gradually saturates after 19 cycles, suggesting a progressive phase transition or improved homogeneity of the sample. To assess the SHG performance of 1M-WS_2, we exfoliated a 2M-WS_2 sample to a thickness of 2.2 nm (~3 layers), ensuring the laser beam could pass through the sample for a homogeneous phase transition. We observe an intriguing phenomenon where the phase transition occurs within a specific thickness range, from 3 layers (2.4 nm) to approximately 100 layers (~80 nm) (a detailed explanation is provided in Supporting Information Section 2). For comparison, we also measured the SHG performance of exfoliated monolayer (ML) MoS_2 as a reference to accurately calculate the second-order nonlinear susceptibility ($\chi^{(2)}$) of 1M-WS_2. The SHG spectra for both samples are shown in Figure 2c, where the intensity of ML MoS_2 is scaled by a factor of 1000 for clarity. Using the experimental value of $\chi^{(2)}_{1L\text{-}MoS_2}$ (130 pm/V at 1064 nm excitation wavelength), we calculate $\chi^{(2)}_{1M\text{-}WS_2}$ to be 2362 pm/V. This value is a record for 2D materials as far as we know, surpassing even the recently reported $NbIO_2$ under external electric field excitation.[15] Besides, a direct measurement is carried out by collecting the intensity of the SHG signal, which shows a $\chi^{(2)}_{1M\text{-}WS_2}$ of 1830 pm/V, aligning well with the reference sample method mentioned above (detailed in Supporting Information Section 3). We also measured the excitation power dependence of SHG intensity. A clear linear relationship between SHG intensity and excitation power is observed on a log−log scale, as shown in Figure 2d. The fitted slope of 1.92 is consistent with the expected quadratic dependence of SHG on excitation power.

Previous studies have consistently reported the transformation of the 2M phase directly to the ground-state centrosymmetric 2H phase. We replicate these results using a femtosecond laser with an excitation wavelength of 1064 nm to compare with our picosecond laser experiments. As shown in Figures S4 and S5, the femtosecond laser-treated 2M-WS_2 sample does not induce any SHG signal. This observation indicates that the photoinduced phase transition is a light-intensity-dependent process. While femtosecond laser excitation primarily stabilizes the thermodynamically stable centrosymmetric phase, picosecond laser excitation promotes the formation of a metastable state without inversion symmetry, resulting in remarkable nonlinear optical properties. The contrasting phase transition results induced by femtosecond and picosecond lasers arise from differences in peak intensity and pulse duration. Under femtosecond laser

https://doi.org/10.1021/acs.nanolett.5c00536
Nano Lett. 2025, 25, 5821−5827

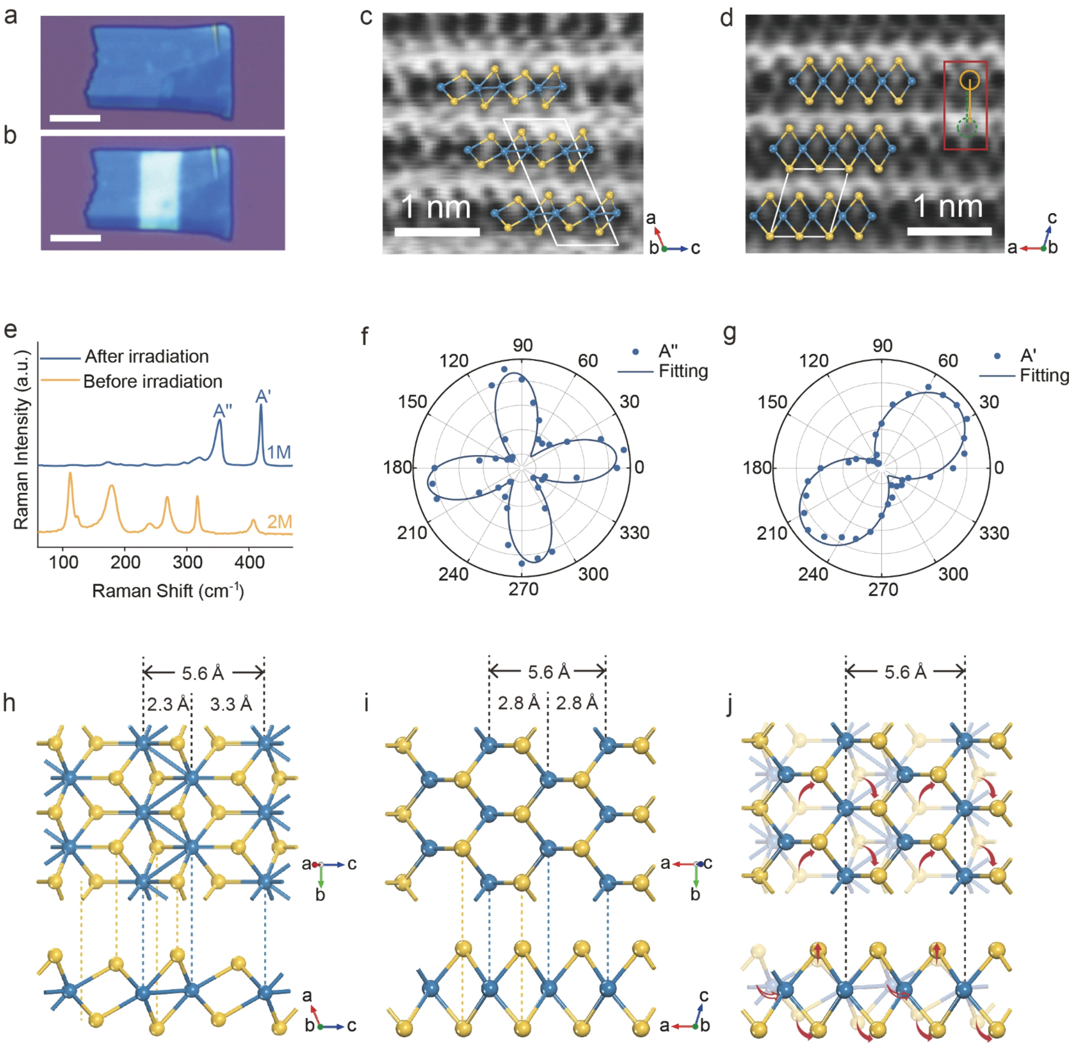

Figure 3. Metastable phase transition pathway. (a, b) Optical images of the thin flake (~26 nm) before and after laser irradiation. The irradiated area is indicated by the region where color changes occur. Scale bar, 5 μm. (c, d) Bright-field scanning transmission electron microscopy (BF-STEM) images of 2M-WS_2 and 1M-WS_2 along the [010] direction, with their respective crystal structures superimposed. Open yellow and green circles denote the atomic positions of W and S in adjacent layers. (e) Raman spectra of 2M-WS_2 and 1M-WS_2, showing two characteristic vibrational modes at 350 cm^{-1} (A″) and 410 cm^{-1} (A′). (f, g) Angle-dependent Raman scattering intensities of the A″ and A′ modes of 1M-WS_2 under a parallel configuration. (h-j) Crystal structures of 2M-WS_2 and 1M-WS_2, along with an illustration of their atomic evolution during the phase transition.

excitation, the ultrashort pulse duration enables energy to be delivered into the material within an extremely short time scale, resulting in an exceptionally high peak power density. This creates a transient high-energy state that allows the system to overcome higher energy barriers, bypass intermediate metastable states, and transition directly into the thermodynamically most stable phase. In contrast, picosecond laser irradiation, with its relatively longer pulse duration and lower peak energy, leads to slower energy accumulation. This facilitates a phase transition through a metastable pathway, resulting in the formation of a metastable state rather than the thermodynamically stable phase. By controlling the excitation power, we can selectively achieve different metastable materials that are inaccessible through conventional synthesis routes.

The giant enhancement in SHG susceptibility, which is ten times higher than that of CVD-grown 3R-WS_2,[38] suggests the emergence of a novel structural configuration. To investigate this, we conducted a detailed structural characterization using bright-field scanning transmission electron microscopy (BF-STEM). Figures 3a and 3b show optical images of the sample before and after the phase transition, respectively. The two-ends of the sample were masked to expose only the central region. The observed color change in the sample results from variations in light transmittance, which are caused by changes in conductivity. Figure 3c shows the atomic arrangement of the initial 2M-WS_2 along the [010] direction, while the irradiated area shown in Figure 3d appears to resemble the 3R phase at first glance. Upon closer examination, we find that the position of W atoms aligns with that of the 3R phase, while the S atoms exhibit additional transverse displacement. This structural distortion can be distinguished from the 3R phase by the slight mismatch between the W and S atoms in adjacent layers, as shown in the orange and green dashed circles in the red box of Figure 3d. In the 3R phase, the positions of these atoms would be vertically aligned. A detailed statistical analysis of the distortion is provided in Figures S6 and S7. These observations indicate a structural distortion and symmetry reduction from rhombohedral to monoclinic phase.

https://doi.org/10.1021/acs.nanolett.5c00536
Nano Lett. 2025, 25, 5821−5827

To confirm the structural distortion relative to the 3R phase, we employed polarized Raman spectroscopy, which is sensitive to crystalline symmetry. Figure 3e shows the Raman spectra of the sample before and after laser irradiation. Prior to irradiation, the Raman spectrum exhibits characteristic modes of 2M-WS_2. After irradiation, the Raman peaks of 2M-WS_2 disappear completely and are replaced by a new set of peaks, indicating a phase transition. The two most prominent peaks are labeled as A″ and A′. Although these peaks also correspond to characteristic phonon modes in the 3R phase, group analysis suggests a circular (angle-independent) polarized resolved spectra for both 3R and 2H phases, but with 4-fold and 2-fold symmetries for the A″ and A′ once the C_3 symmetry is broken (see Supporting Information Section 8 for a detailed analysis). Figures 3f and 3g show the angle-dependent Raman scattering intensities of A″ and A′ under parallel configuration. The 4-fold and 2-fold symmetries of these peaks are consistent with the space group *Cm*.

The newly acquired 1M-WS_2 can be viewed as a distorted 3R phase. Detailed structural evolution is illustrated in Figures 3h−3j. For 2M-WS_2, the distances between two adjacent W atoms are 2.3 Å and 3.3 Å, which aligns well with our STEM observations. In contrast, in 1M-WS_2, the W and S atoms form a distorted trigonal prismatic configuration, with the distances between neighboring W atoms being consistently around 2.8 Å. Upon picosecond laser irradiation, the W−W chains in the 2M phase break, while the distance between W atoms at 5.6 Å remains almost constant, causing the neighboring W atoms to shift, as indicated by the red hollow arrows. Simultaneously, the S atoms break their original W−S covalent bonds and form new bonds, resulting in the distorted trigonal prismatic configuration.

We summarize the second-order nonlinear susceptibility of 1M-WS_2 ($\chi^{(2)}_{\text{1M-WS}_2}$) as a function of excitation wavelength (raw data shown in Figure S10) in in Figure 4, alongside several other nonlinear 2D materials.[39−43] For a fair comparison, we only included values from experiments that utilized reference samples, such as MoS_2, to eliminate inconsistencies rising from different experimental methods. As far as we know, the second-order nonlinear susceptibility $\chi^{(2)}_{\text{1M-WS}_2}$ ranks among the highest in 2D materials. Our theoretical calculations based on the distorted structure, shown as the broken black curve in Figure 4, further confirm the exceptional SHG susceptibility, highlighting the importance of structural distortion from the 3R phase.

Recent advances in optically modified 2D materials have focused on multiple systems, where the photoinduced defect, carrier dynamic change, transient symmetry switching, and phase transition plays a key role. For instance, fs laser-induced sulfur vacancies in MoS_2 have been shown to enhance third-harmonic generation (THG) by 50-fold and SHG by 3.3-fold, facilitated by midgap defect states that enable resonant nonlinear processes.[44] Dynamic carrier modulation, as demonstrated in graphene, achieves >90% THG modulation within 2.5 ps by photoexcited hot carriers altering nonlinear susceptibility.[45] Additionally, light-induced symmetry switch in materials, such as WTe_2,[46] $MoTe_2$,[47] and $ZrTe_5$,[48] enables ultrafast modified nonlinear optical responses and topological properties by dynamically switching inversion symmetry. In our work, photoinduced phase transition achieves a giant SHG response in a novel noncentrosymmetric 1M-WS_2, obtained through ps laser irradiation of the centrosymmetric 2M-WS_2.

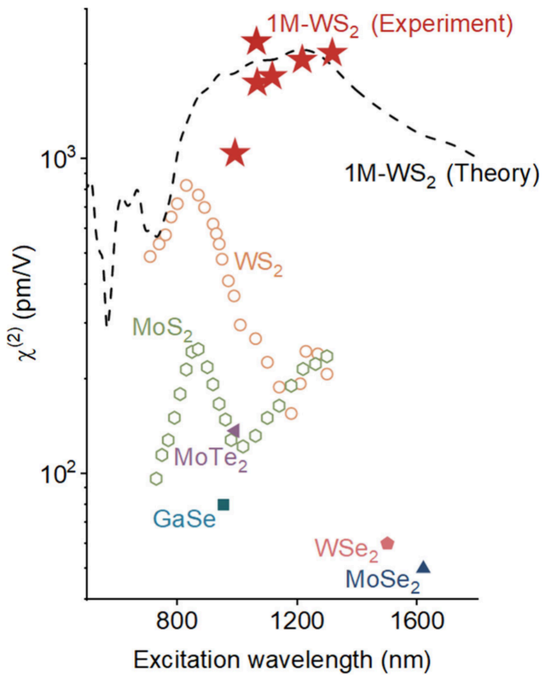

Figure 4. Comparison of the second-order nonlinear susceptibility ($\chi^{(2)}$) between 1M-WS_2 and other 2D materials, including experimental values for MoS_2,[39] WS_2,[39] 1T′-$MoTe_2$,[40] WSe_2,[41] $MoSe_2$,[42] and GaSe,[43] all normalized to monolayer values. The theoretical calculation for 1M-WS_2 is represented by the black dashed curve.

Optical modification serves as an effective approach to tuning the nonlinear optical properties of 2D materials, offering new opportunities for their applications in photonic devices and quantum optics.

To conclude, we introduce a photoinduced approach to achieve a giant SHG response in a novel noncentrosymmetric 1M-WS_2 phase. We observe an intriguing light-intensity-selective structural transformation pathways, each associated with distinct physical properties. The intrinsic 2D nature and moisture robustness of 1M-WS_2 offer significant potential for integrating additional tuning strategies, such as gating and twisting, to achieve an even higher nonlinear susceptibility and energy conversion efficiency, paving the way for compact optical devices.

EXPERIMENTAL SECTION

Sample Fabrication. $K_{0.7}WS_2$ single crystals were synthesized by a solid-state reaction at first.[49] The K, W and S were mixed stoichiometrically in an alumina crucible and then sealed in a vacuum silica tube. $K_{0.7}WS_2$ single crystals were obtained by slowly heating the mixture to 1123 K and keeping this temperature for 24 h, and then cooling it to 823 K in 3000 min. 2M-WS_2 single crystals were prepared by stirring the obtained $K_{0.7}WS_2$ in acid potassium dichromate solution for 2 h.

Few-layer 2M-WS_2 samples were prepared by exfoliating thin flakes from the bulk crystal with scotch tape and transferring them onto a SiO_2 (300 nm)/Si substrate using a water-free PDMS stamp technique. The flake thickness was characterized by atomic force microscopy (AFM) using a Bruker Multimode 8 system.

Laser Irradiation. Picosecond laser irradiation was carried out using a Nd:YAG laser (EKSPLA PL2210A) operating at a wavelength of 1064 nm. The laser parameters were configured as follows: spot diameter of 3 mm, pulse energy of 300 μJ, pulse duration of 25 ps, and repetition rate of 1 kHz. For femtosecond laser irradiation, a femtosecond laser system comprising a laser oscillator, an amplifier, and an optical parametric amplifier (OPA) was used. The system included a Mai Tai SP Ti:sapphire femtosecond oscillator (Spectra-Physics, USA) with a tuning range from 750 to 850 nm, pulse duration of less than 120 fs, repetition rate of 1 kHz, and average power of 1 W at 800 nm. The laser output was amplified using a Spitfire Ace 1001HP Ti:sapphire amplifier (Spectra-Physics, USA), achieving a pulse energy of 7 mJ at 800 nm while maintaining a pulse duration of less than 120 fs and a repetition rate of 1 kHz. Wavelength extension was enabled by a Topas-Prime OPA (Spectra-Physics, USA), providing a tuning range from 480 nm to 11 μm with an output energy of 7 mJ at 800 nm and a repetition rate of 1 kHz. For fs-laser irradiation of the sample, we adopt the following laser parameters: spot diameter of 1 mm, excitation power of 2, 2.5, 3, 3.5, and 4 mW, excitation wavelength of 1064 nm, pulse duration of 120 fs, and a repetition rate of 1 kHz.

STEM Measurements. Cross-sectional microscopy samples were prepared through focused ion beam (FIB) milling. Atomic-scale HAADF-STEM imaging was conducted using a Cs-corrected JEM ARM200CF microscope operating at 200 kV. A high-angle annular detector was utilized for Z-contrast imaging, with a beam convergence angle of 28.5 mrad and a collection angle ranging from 90 to 370 mrad.

Raman Measurements. Raman spectra were performed by using a confocal microscope (WITec, alpha 300R) with an excitation wavelength of 532 nm, a 100× objective, and an 1800-groove mm^{-1} grating. Angle-resolved Raman scattering intensity was measured by simultaneously rotating the half-wave slice in the common optical path of the incident laser and scattered light and the analyzer in front of the spectrometer. The parallel configuration was used in the experiments.

SHG Measurements. SHG measurements with the excitation wavelength at 1064 nm were performed using a confocal microscope (WITec, alpha-300) equipped with a laser at 1064 nm excitation wavelength (Rainbow 1064 OEM, with wavelength of 1064 nm, pulse duration of 15 ps and repetition rate of 50 MHz). A 100× objective (about 0.5 μm spot size) and a 600-groove mm-1 grating is employed to attain SHG signals of samples. The SHG measurements with different excitation wavelengths were performed using a femtosecond laser combined with a collinear optical parametric amplifier (OPA). The femtosecond laser (Pharos 2, Light Conversion) was operated with the following parameters: a pump energy of 180 μJ, a repetition rate of 100 kHz, a central wavelength of 1030 nm, and a pulse duration of 224 fs. The OPA (ORPHEUS-HP, Light Conversion) was used to tune the excitation wavelength across a range of 800 nm to 2 μm. The laser beam was focused on the sample using a 50x objective lens, and the SHG signal was collected in a reflection geometry.

SHG Theoretical Calculations. The second harmonic susceptibility was calculated using the independent-particle approximation,[50] as implemented in the ABINIT software package,[51] which employs a plane-wave basis set. The calculations utilized projector-augmented wave (PAW) potentials in conjunction with the Perdew−Burke−Ernzerhof (PBE) exchange-correlation functional.[52] A plane-wave energy cutoff of 800 eV was adopted, and the Brillouin zone was sampled with a dense 32 × 32 × 16 k-point grid. Furthermore, a scissor shift was applied to the bandgap calculated with the Heyd−Scuseria−Ernzerhof (HSE) hybrid functional.[53]

■ ASSOCIATED CONTENT

Supporting Information

The Supporting Information is available free of charge at https://pubs.acs.org/doi/10.1021/acs.nanolett.5c00536.

> Additional characterization and analytical data including evolution of SHG intensities with laser irradiation cycles at different ps laser pulse energies, thickness limit for the ps laser-induced phase transition, second-order nonlinear susceptibility calculation, fs laser-treated 2M-WS_2, STEM of 1M-WS_2, Raman spectra for different ps laser pulse cycles, polarized Raman analysis, SHG conversion efficiency under different experimental conditions, SHG behavior of 1M-WS_2 at different wavelengths, and the thickness of samples determined by AFM (PDF)

■ AUTHOR INFORMATION

Corresponding Authors

Jian-gang Guo − *Beijing National Laboratory for Condensed Matter Physics, Institute of Physics, Chinese Academy of Sciences, Beijing 100190, China;* orcid.org/0000-0003-3880-3012; Email: jgguo@iphy.ac.cn

Tianping Ying − *Beijing National Laboratory for Condensed Matter Physics, Institute of Physics, Chinese Academy of Sciences, Beijing 100190, China;* orcid.org/0000-0001-7665-1270; Email: ying@iphy.ac.cn

Xiaolong Chen − *Beijing National Laboratory for Condensed Matter Physics, Institute of Physics, Chinese Academy of Sciences, Beijing 100190, China; School of Physical Sciences, University of Chinese Academy of Sciences, Beijing 100049, China; Songshan Lake Materials Laboratory, Dongguan 523808, China;* orcid.org/0000-0001-8455-2117; Email: xlchen@iphy.ac.cn

Authors

Xinyue Li − *Beijing National Laboratory for Condensed Matter Physics, Institute of Physics, Chinese Academy of Sciences, Beijing 100190, China; School of Physical Sciences, University of Chinese Academy of Sciences, Beijing 100049, China*

Boqin Song − *Beijing National Laboratory for Condensed Matter Physics, Institute of Physics, Chinese Academy of Sciences, Beijing 100190, China;* orcid.org/0009-0007-3323-8583

Jiahao Yan − *Beijing National Laboratory for Condensed Matter Physics, Institute of Physics, Chinese Academy of Sciences, Beijing 100190, China; School of Integrated Circuits and Electronics, Beijing Institute of Technology, Beijing 100081, China*

Haijun Cao − *Beijing National Laboratory for Condensed Matter Physics, Institute of Physics, Chinese Academy of Sciences, Beijing 100190, China; School of Physical Sciences, University of Chinese Academy of Sciences, Beijing 100049, China*

Tongtong Xue − *Advanced Research Institute of Multidisciplinary Sciences, Beijing Institute of Technology, Beijing 100081, China*

https://doi.org/10.1021/acs.nanolett.5c00536
Nano Lett. 2025, 25, 5821−5827

Jing Chen − *Beijing National Laboratory for Condensed Matter Physics, Institute of Physics, Chinese Academy of Sciences, Beijing 100190, China*
Yunyun Dai − *Advanced Research Institute of Multidisciplinary Sciences, Beijing Institute of Technology, Beijing 100081, China;* orcid.org/0000-0002-1186-1864
Luojun Du − *Beijing National Laboratory for Condensed Matter Physics, Institute of Physics, Chinese Academy of Sciences, Beijing 100190, China*
Qinghua Zhang − *Beijing National Laboratory for Condensed Matter Physics, Institute of Physics, Chinese Academy of Sciences, Beijing 100190, China*
Sheng Meng − *Beijing National Laboratory for Condensed Matter Physics, Institute of Physics, Chinese Academy of Sciences, Beijing 100190, China;* orcid.org/0000-0002-1553-1432

Complete contact information is available at:
https://pubs.acs.org/10.1021/acs.nanolett.5c00536

Author Contributions

X.L. and B.S. contributed equally. J.G., T.Y., and X.C. conceptualized the idea and provided project supervision. X.L. synthesized the samples. X.L., J.Y., T.X., and Y.D. performed the SHG measurements. X.L. performed the Raman measurements with the help of L.D. J.C. and Q.Z. performed the STEM measurements. H.C. and S.M. performed the theoretical calculations. X.L., B.S., J.G., and T.Y. analyzed the data and wrote the paper, with input from all authors.

Notes

The authors declare no competing financial interest.

■ ACKNOWLEDGMENTS

We thank Yuan Lin for the discussion of experimental results, Xu Liu for theoretical calculations and Jinghan Zhao for data analysis of SHG. This work was financially supported by the National Natural Science Foundation of China (grants 52250308), National Key Research and Development Program of China (grants 2021YFA1401800 and 2023YFA1406301). A portion of numerical computations were carried out at the Hefei Advanced Computing Center.

■ REFERENCES

(1) Shen, Y. R. *The Principles of Nonlinear Optics*; Wiley: 2003.
(2) Shen, Y. R. Surface Properties Probed by Second-Harmonic and Sum-Frequency Generation. *Nature* **1989**, *337* (6207), 519−525.
(3) Hsieh, D.; McIver, J. W.; Torchinsky, D. H.; Gardner, D. R.; Lee, Y. S.; Gedik, N. Nonlinear Optical Probe of Tunable Surface Electrons on a Topological Insulator. *Phys. Rev. Lett.* **2011**, *106* (5), 057401.
(4) Yin, X.; Ye, Z.; Chenet, D. A.; Ye, Y.; Hone, J. C.; Zhang, X. Edge Nonlinear Optics on a MoS_2 Atomic Monolayer. *Science* **2014**, *344*, 488−490.
(5) Li, X.; Qiu, T.; Zhang, J.; Baldini, E.; Lu, J.; Rappe, A. M.; Nelson, K. A. Terahertz Field−Induced Ferroelectricity in Quantum Paraelectric $SrTiO_3$. *Science* **2019**, *364* (6445), 1079−1082.
(6) Lu, J.; Luo, R.; Zhou, J.; Hao, M.; Chai, C.; Ying, T.; Gao, Y.; Jin, S.; Chen, X. High, Multiple, and Nonvolatile Polarizations in Organic−Inorganic Hybrid $[(CH_3)_3(CH_2CH_2Cl)N]_2InCl_5{\cdot}H_2O$ for Memcapacitor. *J. Am. Chem. Soc.* **2024**, *146* (1), 281−288.
(7) Luo, M.; Li, X.; Jiang, X.; Lin, Z.; Zhou, Z. The Compatibly Large Nonlinear Optical Effect and High Laser-Induced Damage Threshold in a Thiophosphate $CsInP_2S_7$ Constructed with $[P_2S_7]^{4-}$ and $[InS_6]^{9-}$. *Chinese Chem. lett.* **2024**, *35* (1), 109108.
(8) Malard, L. M.; Alencar, T. V.; Barboza, A. P. M.; Mak, K. F.; De Paula, A. M. Observation of Intense Second Harmonic Generation from MoS_2 Atomic Crystals. *Phys. Rev. B* **2013**, *87* (20), 201401.
(9) Clark, D. J.; Senthilkumar, V.; Le, C. T.; Weerawarne, D. L.; Shim, B.; Jang, J. I.; Shim, J. H.; Cho, J.; Sim, Y.; Seong, M.-J.; Rhim, S. H.; Freeman, A. J.; Chung, K.-H.; Kim, Y. S. Strong Optical Nonlinearity of CVD-Grown MoS_2 Monolayer as Probed by Wavelength-Dependent Second-Harmonic Generation. *Phys. Rev. B* **2014**, *90* (12), 121409.
(10) Zhou, X.; Cheng, J.; Zhou, Y.; Cao, T.; Hong, H.; Liao, Z.; Wu, S.; Peng, H.; Liu, K.; Yu, D. Strong Second-Harmonic Generation in Atomic Layered GaSe. *J. Am. Chem. Soc.* **2015**, *137* (25), 7994−7997.
(11) Chen, X.; Fei, G.; Song, Y.; Ying, T.; Huang, D.; Pan, B.; Yang, D.; Yang, X.; Chen, K.; Zhan, X.; Wang, J.; Zhang, Q.; Li, Y.; Gu, L.; Gou, H.; Chen, X.; Li, S.; Cheng, J.; Liu, X.; Hosono, H.; Guo, J.; Chen, X. Superatomic-Charge-Density-Wave in Cluster-Assembled $Au_6Te_{12}Se_8$ Superconductors. *J. Am. Chem. Soc.* **2022**, *144* (45), 20915−20922.
(12) Chen, K.; Pan, J.; Yin, W.; Ma, C.; Wang, L. Flexible Electronics Based on One-Dimensional Inorganic Semiconductor Nanowires and Two-Dimensional Transition Metal Dichalcogenides. *Chinese Chem. lett.* **2023**, *34* (11), 108226.
(13) Xie, Z.; Luo, R.; Ying, T.; Gao, Y.; Song, B.; Yu, T.; Chen, X.; Hao, M.; Chai, C.; Yan, J.; Huang, Z.; Chen, Z.; Du, L.; Zhu, C.; Guo, J.; Chen, X. Dynamic-to-Static Switch of Hydrogen Bonds Induces a Metal−Insulator Transition in an Organic−Inorganic Superlattice. *Nat. Chem.* **2024**, *16* (11), 1803−1810.
(14) Liang, J.; Zhang, J.; Li, Z.; Hong, H.; Wang, J.; Zhang, Z.; Zhou, X.; Qiao, R.; Xu, J.; Gao, P.; Liu, Z.; Liu, Z.; Sun, Z.; Meng, S.; Liu, K.; Yu, D. Monitoring Local Strain Vector in Atomic-Layered $MoSe_2$ by Second-Harmonic Generation. *Nano Lett.* **2017**, *17* (12), 7539−7543.
(15) Abdelwahab, I.; Tilmann, B.; Wu, Y.; Giovanni, D.; Verzhbitskiy, I.; Zhu, M.; Berté, R.; Xuan, F.; Menezes, L. de S.; Eda, G.; Sum, T. C.; Quek, S. Y.; Maier, S. A.; Loh, K. P. Giant Second-Harmonic Generation in Ferroelectric $NbOI_2$. *Nat. Photonics* **2022**, *16* (9), 644−650.
(16) Puri, S.; Patel, S.; Cabellos, J. L.; Rosas-Hernandez, L. E.; Reynolds, K.; Churchill, H. O. H.; Barraza-Lopez, S.; Mendoza, B. S.; Nakamura, H. Substrate Interference and Strain in the Second-Harmonic Generation from $MoSe_2$ Monolayers. *Nano Lett.* **2024**, *24* (41), 13061−13067.
(17) Wang, J.; Han, N.; Luo, Z.-D.; Zhang, M.; Chen, X.; Liu, Y.; Hao, Y.; Zhao, J.; Gan, X. Electrically Tunable Second Harmonic Generation in Atomically Thin ReS_2. *ACS Nano* **2022**, *16* (4), 6404−6413.
(18) Hong, H.; Wu, C.; Zhao, Z.; Zuo, Y.; Wang, J.; Liu, C.; Zhang, J.; Wang, F.; Feng, J.; Shen, H.; Yin, J.; Wu, Y.; Zhao, Y.; Liu, K.; Gao, P.; Meng, S.; Wu, S.; Sun, Z.; Liu, K.; Xiong, J. Giant Enhancement of Optical Nonlinearity in Two-Dimensional Materials by Multiphoton-Excitation Resonance Energy Transfer from Quantum Dots. *Nat. Photonics* **2021**, *15* (7), 510−515.
(19) Hong, H.; Huang, C.; Ma, C.; Qi, J.; Shi, X.; Liu, C.; Wu, S.; Sun, Z.; Wang, E.; Liu, K. Twist Phase Matching in Two-Dimensional Materials. *Phys. Rev. Lett.* **2023**, *131* (23), 233801.
(20) Yao, K.; Finney, N. R.; Zhang, J.; Moore, S. L.; Xian, L.; Tancogne-Dejean, N.; Liu, F.; Ardelean, J.; Xu, X.; Halbertal, D.; Watanabe, K.; Taniguchi, T.; Ochoa, H.; Asenjo-Garcia, A.; Zhu, X.; Basov, D. N.; Rubio, A.; Dean, C. R.; Hone, J.; Schuck, P. J. Enhanced Tunable Second Harmonic Generation from Twistable Interfaces and Vertical Superlattices in Boron Nitride Homostructures. *Sci. Adv.* **2021**, *7* (10), No. eabe8691.
(21) Fan, X.; Jiang, Y.; Zhuang, X.; Liu, H.; Xu, T.; Zheng, W.; Fan, P.; Li, H.; Wu, X.; Zhu, X.; Zhang, Q.; Zhou, H.; Hu, W.; Wang, X.; Sun, L.; Duan, X.; Pan, A. Broken Symmetry Induced Strong Nonlinear Optical Effects in Spiral WS_2 Nanosheets. *ACS Nano* **2017**, *11* (5), 4892−4898.
(22) Hsu, W.-T.; Zhao, Z.-A.; Li, L.-J.; Chen, C.-H.; Chiu, M.-H.; Chang, P.-S.; Chou, Y.-C.; Chang, W.-H. Second Harmonic

Generation from Artificially Stacked Transition Metal Dichalcogenide Twisted Bilayers. *ACS Nano* **2014**, *8* (3), 2951−2958.

(23) Beaurepaire, E.; et al. Ultrafast Spin Dynamics in Ferromagnetic Nickel. *Phys. Rev. Lett.* **1996**, *76* (22), 4250−4253.

(24) Kirilyuk, A.; Kimel, A. V.; Rasing, T. Ultrafast Optical Manipulation of Magnetic Order. *Rev. Mod. Phys.* **2010**, *82* (3), 2731−2784.

(25) Disa, A. S.; Fechner, M.; Nova, T. F.; Liu, B.; Först, M.; Prabhakaran, D.; Radaelli, P. G.; Cavalleri, A. Polarizing an Antiferromagnet by Optical Engineering of the Crystal Field. *Nat. Phys.* **2020**, *16* (9), 937−941.

(26) Nova, T. F.; Disa, A. S.; Fechner, M.; Cavalleri, A. Metastable Ferroelectricity in Optically Strained $SrTiO_3$. *Science* **2019**, *364* (6445), 1075−1079.

(27) Collet, E.; Lemée-Cailleau, M.-H.; Buron-Le Cointe, M.; Cailleau, H.; Wulff, M.; Luty, T.; Koshihara, S.-Y.; Meyer, M.; Toupet, L.; Rabiller, P.; Techert, S. Laser-Induced Ferroelectric Structural Order in an Organic Charge-Transfer Crystal. *Science* **2003**, *300* (5619), 612−615.

(28) Mankowsky, R.; Von Hoegen, A.; Först, M.; Cavalleri, A. Ultrafast Reversal of the Ferroelectric Polarization. *Phys. Rev. Lett.* **2017**, *118* (19), 197601.

(29) Xu, X.; Wang, T.; Chen, P.; Zhou, C.; Ma, J.; Wei, D.; Wang, H.; Niu, B.; Fang, X.; Wu, D.; Zhu, S.; Gu, M.; Xiao, M.; Zhang, Y. Femtosecond Laser Writing of Lithium Niobate Ferroelectric Nanodomains. *Nature* **2022**, *609* (7927), 496−501.

(30) Fausti, D.; Tobey, R. I.; Dean, N.; Kaiser, S.; Dienst, A.; Hoffmann, M. C.; Pyon, S.; Takayama, T.; Takagi, H.; Cavalleri, A. Light-Induced Superconductivity in a Stripe-Ordered Cuprate. *Science* **2011**, *331* (6014), 189−191.

(31) Mitrano, M.; Cantaluppi, A.; Nicoletti, D.; Kaiser, S.; Perucchi, A.; Lupi, S.; Di Pietro, P.; Pontiroli, D.; Riccò, M.; Clark, S. R.; Jaksch, D.; Cavalleri, A. Possible Light-Induced Superconductivity in K_3C_{60} at High Temperature. *Nature* **2016**, *530* (7591), 461−464.

(32) Buzzi, M.; Nicoletti, D.; Fechner, M.; Tancogne-Dejean, N.; Sentef, M. A.; Georges, A.; Biesner, T.; Uykur, E.; Dressel, M.; Henderson, A.; Siegrist, T.; Schlueter, J. A.; Miyagawa, K.; Kanoda, K.; Nam, M.-S.; Ardavan, A.; Coulthard, J.; Tindall, J.; Schlawin, F.; Jaksch, D.; Cavalleri, A. Photomolecular High-Temperature Superconductivity. *Phys. Rev. X* **2020**, *10* (3), 031028.

(33) Wall, S.; Yang, S.; Vidas, L.; Chollet, M.; Glownia, J. M.; Kozina, M.; Katayama, T.; Henighan, T.; Jiang, M.; Miller, T. A.; Reis, D. A.; Boatner, L. A.; Delaire, O.; Trigo, M. Ultrafast Disordering of Vanadium Dimers in Photoexcited VO_2. *Science* **2018**, *362* (6414), 572−576.

(34) Cho, S.; Kim, S.; Kim, J. H.; Zhao, J.; Seok, J.; Keum, D. H.; Baik, J.; Choe, D.-H.; Chang, K. J.; Suenaga, K.; Kim, S. W.; Lee, Y. H.; Yang, H. Phase Patterning for Ohmic Homojunction Contact in $MoTe_2$. *Science* **2015**, *349* (6248), 625−628.

(35) Guan, Y.; Ding, Y.; Fang, Y.; Wang, G.; Zhao, S.; Wang, L.; Huang, J.; Chen, M.; Hao, J.; Xu, C.; Zhen, L.; Huang, F.; Li, Y.; Yang, L. Femtosecond Laser-Driven Phase Engineering of WS_2 for Nano-Periodic Phase Patterning and Sub-ppm Ammonia Gas Sensing. *Small* **2023**, *19* (45), 2303654.

(36) Yu, Y.; Nam, G.-H.; He, Q.; Wu, X.-J.; Zhang, K.; Yang, Z.; Chen, J.; Ma, Q.; Zhao, M.; Liu, Z.; Ran, F.-R.; Wang, X.; Li, H.; Huang, X.; Li, B.; Xiong, Q.; Zhang, Q.; Liu, Z.; Gu, L.; Du, Y.; Huang, W.; Zhang, H. High Phase-Purity 1T′-MoS_2- and 1T′-$MoSe_2$-Layered Crystals. *Nat. Chem.* **2018**, *10* (6), 638−643.

(37) Liu, Q. M.; Wu, D.; Li, Z. A.; Shi, L. Y.; Wang, Z. X.; Zhang, S. J.; Lin, T.; Hu, T. C.; Tian, H. F.; Li, J. Q.; Dong, T.; Wang, N. L. Photoinduced Multistage Phase Transitions in Ta_2NiSe_5. *Nat. Commun.* **2021**, *12* (1), 2050.

(38) Du, L.; Tang, J.; Liang, J.; Liao, M.; Jia, Z.; Zhang, Q.; Zhao, Y.; Yang, R.; Shi, D.; Gu, L.; Xiang, J.; Liu, K.; Sun, Z.; Zhang, G. Giant Valley Coherence at Room Temperature in 3R WS_2 with Broken Inversion Symmetry. *Research* **2019**, *2019*, 6494565.

(39) Bredillet, K.; Riporto, J.; Forcherio, G. T.; Dunklin, J. R.; Wolf, J.-P.; Bonacina, L.; Mugnier, Y.; Le Dantec, R. Dispersion of the Nonlinear Susceptibility of MoS_2 and WS_2 from Second-Harmonic Scattering Spectroscopy. *Phys. Rev. B* **2020**, *102* (23), 235408.

(40) Beams, R.; Cançado, L. G.; Krylyuk, S.; Kalish, I.; Kalanyan, B.; Singh, A. K.; Choudhary, K.; Bruma, A.; Vora, P. M.; Tavazza, F.; Davydov, A. V.; Stranick, S. J. Characterization of Few-Layer 1T′ $MoTe_2$ by Polarization-Resolved Second Harmonic Generation and Raman Scattering. *ACS Nano* **2016**, *10* (10), 9626−9636.

(41) Rosa, H. G.; Ho, Y. W.; Verzhbitskiy, I.; Rodrigues, M. J. F. L.; Taniguchi, T.; Watanabe, K.; Eda, G.; Pereira, V. M.; Gomes, J. C. V. Characterization of the Second- and Third-Harmonic Optical Susceptibilities of Atomically Thin Tungsten Diselenide. *Sci. Rep.* **2018**, *8* (1), 10035.

(42) Le, C. T.; Clark, D. J.; Ullah, F.; Senthilkumar, V.; Jang, J. I.; Sim, Y.; Seong, M.; Chung, K.; Park, H.; Kim, Y. S. Nonlinear Optical Characteristics of Monolayer $MoSe_2$. *Ann. Phys.-Brlin* **2016**, *528* (7−8), 551−559.

(43) Tang, Y.; Mandal, K. C.; McGuire, J. A.; Lai, C. W. Layer- and Frequency-Dependent Second Harmonic Generation in Reflection from GaSe Atomic Crystals. *Phys. Rev. B* **2016**, *94* (12), 125302.

(44) Akkanen, S.-T. M.; Arias-Muñoz, J. C.; Emelianov, A. V.; Mentel, K. K.; Tammela, J. V.; Partanen, M.; Das, S.; Faisal, A.; Pettersson, M.; Sun, Z. Enhanced Nonlinear Optical Responses in MoS_2 via Femtosecond Laser-Induced Defect-Engineering. *Adv. Funct. Mater.* **2024**, *34* (46), 2406942.

(45) Cheng, Y.; Hong, H.; Zhao, H.; Wu, C.; Pan, Y.; Liu, C.; Zuo, Y.; Zhang, Z.; Xie, J.; Wang, J.; Yu, D.; Ye, Y.; Meng, S.; Liu, K. Ultrafast Optical Modulation of Harmonic Generation in 2D Materials. *Nano Lett.* **2020**, *20* (11), 8053−8058.

(46) Sie, E. J.; Nyby, C. M.; Pemmaraju, C. D.; Park, S. J.; Shen, X.; Yang, J.; Hoffmann, M. C.; Ofori-Okai, B. K.; Li, R.; Reid, A. H.; Weathersby, S.; Mannebach, E.; Finney, N.; Rhodes, D.; Chenet, D.; Antony, A.; Balicas, L.; Hone, J.; Devereaux, T. P.; Heinz, T. F.; Wang, X.; Lindenberg, A. M. An Ultrafast Symmetry Switch in a Weyl Semimetal. *Nature* **2019**, *565* (7737), 61−66.

(47) Zhang, M. Y.; Wang, Z. X.; Li, Y. N.; Shi, L. Y.; Wu, D.; Lin, T.; Zhang, S. J.; Liu, Y. Q.; Liu, Q. M.; Wang, J.; Dong, T.; Wang, N. L. Light-Induced Subpicosecond Lattice Symmetry Switch in $MoTe_2$. *Phys. Rev. X* **2019**, *9* (2), 021036.

(48) Luo, L.; Cheng, D.; Song, B.; Wang, L.-L.; Vaswani, C.; Lozano, P. M.; Gu, G.; Huang, C.; Kim, R. H. J.; Liu, Z.; Park, J.-M.; Yao, Y.; Ho, K.; Perakis, I. E.; Li, Q.; Wang, J. A Light-Induced Phononic Symmetry Switch and Giant Dissipationless Topological Photocurrent in $ZrTe_5$. *Nat. Mater.* **2021**, *20* (3), 329−334.

(49) Fang, Y.; Pan, J.; Zhang, D.; Wang, D.; Hirose, H. T.; Terashima, T.; Uji, S.; Yuan, Y.; Li, W.; Tian, Z.; Xue, J.; Ma, Y.; Zhao, W.; Xue, Q.; Mu, G.; Zhang, H.; Huang, F. Discovery of Superconductivity in 2M WS_2 with Possible Topological Surface States. *Adv. Mater.* **2019**, *31* (30), 1901942.

(50) Sharma, S.; Ambrosch-Draxl, C. Second-Harmonic Optical Response from First Principles. *Phys. Scr.* **2004**, *T109*, 128.

(51) Gonze, X.; Amadon, B.; Anglade, P.-M.; Beuken, J.-M.; Bottin, F.; Boulanger, P.; Bruneval, F.; Caliste, D.; Caracas, R.; Côté, M.; Deutsch, T.; Genovese, L.; Ghosez, Ph.; Giantomassi, M.; Goedecker, S.; Hamann, D. R.; Hermet, P.; Jollet, F.; Jomard, G.; Leroux, S.; Mancini, M.; Mazevet, S.; Oliveira, M. J. T.; Onida, G.; Pouillon, Y.; Rangel, T.; Rignanese, G.-M.; Sangalli, D.; Shaltaf, R.; Torrent, M.; Verstraete, M. J.; Zerah, G.; Zwanziger, J. W. ABINIT: First-Principles Approach to Material and Nanosystem Properties. *Comput. Phys. Commun.* **2009**, *180* (12), 2582−2615.

(52) Jollet, F.; Torrent, M.; Holzwarth, N. Generation of Projector Augmented-Wave Atomic Data: A 71 Element Validated Table in the XML Format. *Comput. Phys. Commun.* **2014**, *185* (4), 1246−1254.

(53) Krukau, A. V.; Vydrov, O. A.; Izmaylov, A. F.; Scuseria, G. E. Influence of the Exchange Screening Parameter on the Performance of Screened Hybrid Functionals. *J. Chem. Phys.* **2006**, *125* (22), 224106.